

Article

Investigation of the Static Performance of Hydrostatic Thrust Bearings Considering Non-Gaussian Surface Topography

Huaiqing Lu ^{1,2} and Zhuxin Tian ^{3,*}

¹ College of Mechanical Engineering, Yellow River Conservancy Technical Institute, Kaifeng 475004, China; luhuaiqing@yrcti.edu.cn

² State Key Laboratory of Digital Manufacturing Equipment and Technology, Huazhong University of Science and Technology, Wuhan 430074, China

³ College of Mechanical and Power Engineering, China Three Gorges University, Yichang 443002, China

* Correspondence: tianzhuxin@ctgu.edu.cn; Tel.: +86-1587-1778-172

Abstract: The dynamic and static characteristics of hydrostatic thrust bearings are significantly affected by the bearing surface topography. Previous studies on hydrostatic thrust bearings have focused on Gaussian distribution models of bearing surface topography. However, based on actual measurements, the non-Gaussianity of the distribution characteristics of bearing surface topography is clear. To accurately characterize the non-Gaussian distribution of bearing surface topography, the traditional probability density function of Gaussian distribution was modified by introducing Edgeworth expansion. The non-Gaussian surface was then reflected by two parameters: kurtosis and skewness. This had an effect on the static characteristics of hydrostatic thrust bearings with both circumferential and radial surface topographies. The comparison between the Gaussian distribution results and those of the non-Gaussian model showed that errors between the two models could reach more than 10%. Therefore, it is important to take into account the non-Gaussianity of bearing surface when discussing static characteristics of hydrostatic thrust bearings considering the surface topography.

Keywords: hydrostatic thrust bearings; surface topography; non-Gaussianity; static performance; kurtosis and skewness



Citation: Lu, H.; Tian, Z.

Investigation of the Static Performance of Hydrostatic Thrust Bearings Considering Non-Gaussian Surface Topography. *Lubricants* **2023**, *11*, 267. <https://doi.org/10.3390/lubricants11060267>

Received: 18 May 2023

Revised: 7 June 2023

Accepted: 15 June 2023

Published: 20 June 2023



Copyright: © 2023 by the authors. Licensee MDPI, Basel, Switzerland. This article is an open access article distributed under the terms and conditions of the Creative Commons Attribution (CC BY) license (<https://creativecommons.org/licenses/by/4.0/>).

1. Introduction

Hydrostatic bearings have a number of advantages, such as high loading capacity, stiffness, and low frictional wear, which makes them ideal for heavy and precision mechanical equipment [1]. Thus, hydrostatic bearings are used widely in the spindles of machine tools such as high-precision lathes and grinding machines; optimizing the design of hydrostatic bearings is an important way to improve the performance of machine tools [2,3]. During the rotating process, the bearing surface and the spindle surface are kept apart by an oil film that is typically around 10 μm thick, similar to the fluctuations of the traditional bearing surface topography. As such, the bearing surface topography must be taken into account when discussing the static and dynamic performance of hydrostatic bearings.

Several studies have been conducted in recent decades to investigate the impact of bearing surface topography on the performance of hydrostatic and aerostatic bearings. Song et al. [4] discussed the performance of gas bearings with spiral grooves on the surface, and found that the spiral groove improved the load capacity of bearings. Applying a numerical method, Feng et al. [5] investigated the dynamics of a bearing–rotor system considering grooves of the bearing surface, and discovered that some kinds of grooves could improve the stability of the system. In addition to these studies on the surface grooves of bearings, there have been many statistical investigations on the structures of bearing surfaces. Christensen [6] proposed a statistical model based on Gaussian distribution to characterize the surface topography of bearings, which was then used by

Lin [7] to examine the influence of surface topography on the stiffness and damping characteristics of hydrostatic thrust bearings. The results showed that the bearing surface topography had a significant impact on the stiffness and damping coefficients, and that ignoring it could result in significant errors in the dynamic characteristics of bearings. Walicka et al. [8–10] investigated the effect of surface topography on the static characteristics of hydrostatic thrust bearings lubricated with different types of fluids. Lin [11–13] developed Hopf bifurcating theory and short bearing approximation, and examined the influence of different surface topography structures on the non-linear stability of hydrodynamic bearings, finding that they had a significant impact on the size of upper and lower limit circles of bearings. Naduvinamani et al. [14–17] studied the effect of surface topography on the performance of various sliding support systems, such as bearing rotor systems, annular recess thrust bearings, rectangular recess thrust bearings, and curved circular plates. Jurczak et al. [18] demonstrated the impact of surface topography on the performance of sliding support systems lubricated with Ellis fluid. Zhang et al. [19] optimized the oil film morphology of slide bearings by taking into account the surface topography. Lin et al. [20] investigated the impact of bearing surface topography on the dynamic characteristics of slider bearings lubricated with non-Newtonian fluids. Pang et al. [21] considered the influencing factor of surface topography when analyzing the running noise of bearings. Tian et al. [22] discussed the influence of surface topography on the dynamic characteristics of long journal bearings. Pei et al. [23] determined the influence of surface topography on the characteristics of floating ring bearings and illustrated that the effect of surface topography cannot be ignored.

In the aforementioned studies, it is evident that the surface topography significantly affects the static and dynamic characteristics of hydrostatic and hydrodynamic bearings, and hence cannot be overlooked when discussing bearing performance. However, the surface topographies analyzed in previous studies were typically assumed to follow a Gaussian distribution. In reality, bearing surfaces are typically processed by turning and grinding, and the distribution characteristics of surface topography are found to deviate significantly from the Gaussian distribution, as reported by Peklenik [24] and Li [25] et al. Taking into account the non-Gaussian nature of surface roughness, Tian et al. [26] investigated the threshold speed of short bearings and found that the effect of non-Gaussian surface roughness could not be disregarded. Winkler et al. [27] proposed a numerical model to discuss the abrasion of non-Gaussian surfaces. Ma et al. [28] discussed misaligned hydrodynamic bearings with non-Gaussian surface topography; the results illustrated that there would be obvious errors if the non-Gaussianity of the bearing surface was ignored. Applying the mixed elastohydrodynamic theory, Pei et al. [29] studied the influence of non-Gaussian surface topography on the film thickness of line contact, and established the relationship between the minimum film thickness and non-Gaussian parameters of the surface. Chen et al. [30] examined the dynamic contact performance of non-Gaussian surfaces through fractal theory. Ren et al. [31] investigated the contact performance of non-Gaussian surfaces in engineering applications, and discovered that the contact performance of surfaces was significantly affected by the non-Gaussian parameters. Zhao et al. [32] analyzed the effects of non-Gaussian surface topography on the wear of surfaces in mixed lubrication.

After examining the studies mentioned above, it has been noticed that these investigations predominantly concentrate on the contact performance of surfaces, with little discussion regarding the static performance of hydrostatic thrust bearings when considering non-Gaussian surface topography. When it comes to bearing surfaces processed through turning and grinding, significant deviations from the Gaussian distribution have been observed in the distribution characteristics of surface topography. Therefore, to conduct a more precise analysis of the static characteristics of hydrostatic thrust bearings, it is essential to consider the non-Gaussian nature of the bearing surface topography during the analytical process.

2. Fundamentals and Methods

The Christensen statistical model [6] was applied in this study to illustrate the surface topography. Using this statistical model, there are two kinds of surface topographies for hydrostatic bearings: radial and circumferential topography. For radial topography, the surface texture of the bearing is distributed along the radial direction of the bearing, as shown in Figure 1. For a specified bearing radius, the corresponding region on the bearing surface is a circle. When the bearing surface statistical model is established along the circumferential direction, the circumferential topography is obtained. From the illustrations by Peklenik [24] and Li et al. [25], for bearing surfaces processed by turning and grinding, the distribution characteristics of surface topography significantly deviated from the Gaussian distribution. Thus, the non-Gaussian statistical model was applied in this study to describe the surface topography of bearings.

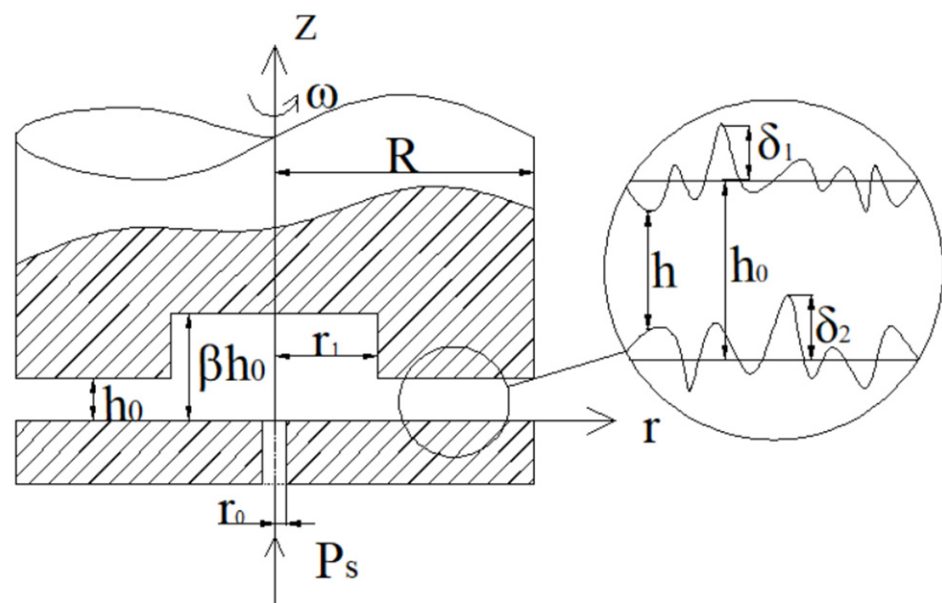


Figure 1. Structure of the thrust bearing.

In Figure 1, the structure of a hydrostatic thrust bearing is displayed; R is the bearing radius, r_1 is the recess radius, r_0 is the radius of the supply hole, P_s is the pressure of supply oil, ω is the rotating speed of the journal, and h_0 and βh_0 are the thickness of oil film in the regions of bearing land and recess in smooth situations, respectively. Additionally, the actual thickness of oil film in the regions of bearing land and recess considering the surface topography could be expressed as follows:

$$h = \beta h_0 + h_s(r, \theta, \xi) \quad 0 < r < r_1 \quad (1)$$

$$h = h_0 + h_s(r, \theta, \xi) \quad r_1 < r < R \quad (2)$$

where $h_s = \delta_1 + \delta_2$ is a random part of the oil film, δ_1 is the variance in the actual journal surface measured from the smooth surface, and δ_2 is the variance in the actual bearing surface measured from the smooth surface. ξ is a random variable representing the surface topography of oil film.

Ignoring the body force of oil film and considering the axial symmetry of the bearing, the motion equations of oil film could be built in the coordinate system in Figure 1 as follows:

$$-\rho \frac{v^2}{r} + \frac{\partial p}{\partial r} = \mu \frac{\partial^2 u}{\partial z^2} \quad (3)$$

$$0 = \frac{\partial^2 v}{\partial z^2} \quad (4)$$

$$\frac{\partial p}{\partial z} = 0 \quad (5)$$

where ρ and μ are the density and viscosity of the lubricant, respectively; r and z are coordinates in the radius direction and vertical direction, respectively; and u and v are the velocities of oil film on radius direction and circumferential direction. With the boundary conditions $v|_{z=0} = 0, v|_{z=h} = r\omega$, the velocity of oil film in the circumferential direction can be found through Equation (4):

$$v = \frac{r\omega}{h}z \quad (6)$$

Substituting Equation (6) into Equation (3), with the boundary condition $u|_{z=0,h} = 0$, the velocity of oil film in the radial direction can be obtained:

$$u = -\frac{\rho r \omega^2}{12\mu h^2}z(z^3 - h^3) + \frac{1}{2\mu} \frac{\partial p}{\partial r}(z-h)z \quad (7)$$

Integrating the expression of u with respect to z from 0 to h , the expression of flow rate Q could be found:

$$\frac{Q}{\pi} = 2r \int_0^h u dz = \frac{1}{20} \frac{\rho r^2 \omega^2 h^3}{\mu} - \frac{h^3 r}{6\mu} \frac{\partial p}{\partial r} \quad (8)$$

The following dimensionless substitution can be introduced:

$$r^* = \frac{r}{R}, p^* = \frac{p}{P_s}, h^* = \frac{h}{h_0}, h_s^* = \frac{h_s}{h_0}, W^* = \frac{W}{\pi R^2 P_s}, Q^* = \frac{6\mu Q}{\pi P_s h_0^3}, S = \frac{3\rho \omega^2 R^2}{20P_s} \quad (9)$$

and the dimensionless expression of flow rate Q^* is

$$Q^* = 2Sr^{*2}h^{*3} - r^*h^{*3} \frac{\partial p^*}{\partial r^*} \quad (10)$$

Taking mathematical expectation of the dimensionless expression of flow rate Q^* :

$$Q_0^* = E(Q^*) = \left(2Sr^{*2} - r^* \frac{\partial p^*}{\partial r^*} \right) q(h^*) \quad (11)$$

where $q(h^*)$ expresses the expected value of h^{*3} . Considering the one-dimensional surface topography of the bearing, $q(h^*)$ is expressed as follows:

$$q(h^*) = \begin{cases} E(h^{*3}) & \text{for radial roughness} \\ E(h^{*-3})^{-1} & \text{for circumferential roughness} \end{cases} \quad (12)$$

operator $E(*)$ expresses the expected value of variable $(*)$, defined as:

$$E(*) = \int_{-\infty}^{+\infty} (*) f(h_s^*) dh_s^* \quad (13)$$

where $f(h_s^*)$ is the probability density function of random variable h_s^* , which is used to display distribution characteristics of the bearing surface topography and could be expressed as:

$$f(h_s^*) = p_n(h_s^*)g(h_s^*) \quad (14)$$

where the probability density function, $g(h_s^*)$, is in a Gaussian distribution as follows:

$$g(h_s^*) = \begin{cases} \frac{35}{32c^7} (c^2 - h_s^{*2})^3, & -c \leq h_s^* \leq c \\ 0, & \text{elsewhere} \end{cases} \quad (15)$$

where c is the half-distribution region of the random variable h_s . The probability density function, $g(h_s)$, terminates at $c = \pm 3\sigma$, and σ is the standard deviation of the random variable h_s . Additionally, $p_n(h_s)$ is the Edgeworth expansion, which was applied to display the non-Gaussian roughness of the bearing surface with two parameters: skewness and kurtosis. Edgeworth expansion is a kind of Chebyshev–Hermite polynomial used to illustrate non-Gaussian distributions. Compared with other expansions, such as Gram–Charlier and Gaussian–Hermite, Edgeworth expansion contains one more Hermit polynomial, while the number of parameters is constant. Therefore, it can not only measure the fitting accuracy, but also has better convergence properties and higher fitting accuracy with more terms in an expansion. The Edgeworth expansion is typically adopted as [25]:

$$p_6(x) = 1 + \frac{s}{6}He_3(x) + \frac{k}{24}He_4(x) + \frac{s^2}{72}He_6(x) \quad (16)$$

where k is the kurtosis of surface roughness distribution reflecting peakedness of the distribution, and s is the skewness of surface roughness distribution reflecting asymmetry of the distribution with respect to the average value. For a Gaussian distribution, the values of kurtosis and skewness are $k = 3$ and $s = 0$, respectively. Additionally, the expressions of Hermite polynomials $He_i(z)$ ($i = 3, 4, 6$) are [33]:

$$\begin{aligned} He_3(x) &= x^3 - 3x \\ He_4(x) &= x^4 - 6x^2 + 3 \\ He_6(x) &= x^6 - 15x^4 + 45x^2 - 3 \end{aligned} \quad (17)$$

Substituting Equation (17) into Equation (16), the Edgeworth expansion of the bearing surface topography could be written as:

$$p_6(h_s^*) = \left(1 + \frac{k-3}{8} - \frac{5s^2}{24}\right) - \frac{s}{2}h_s^* + \left(\frac{5s^2}{8} - \frac{k-3}{4}\right)h_s^{*2} + \frac{s}{6}h_s^{*3} + \left(\frac{k-3}{24} - \frac{5s^2}{24}\right)h_s^{*4} + \frac{s^2}{72}h_s^{*6} \quad (18)$$

Through Equations (12)–(15) and (18), the value of $q(h^*)$ in Equation (11) is obtained, which is determined by three characteristic parameters: c (the half-distribution region of the random variable h_s), k (the kurtosis of surface roughness distribution), and s (the skewness of surface roughness distribution).

Then, the pressure distribution of oil film could be found by solving Equation (11):

$$p_1^* = Sr^{*2} - \frac{Q_0^*}{q(\beta + h_s^*)} \ln r^* + C_1 \quad r_0^* \leq r^* \leq r_1^* \quad (19)$$

$$p_2^* = Sr^{*2} - \frac{Q_0^*}{q(1 + h_s^*)} \ln r^* + C_2 \quad r_1^* \leq r^* \leq 1 \quad (20)$$

where C_1 and C_2 are integration constants, the values of which could be calculated by applying boundary conditions of the pressure distribution $p_1^*|_{r^*=r_0^*} = 1$, $p_1^*|_{r^*=r_1^*} = p_2^*|_{r^*=r_1^*}$ and $p_2^*|_{r^*=1} = 0$:

$$C_1 = 1 - Sr_0^{*2} + \frac{(1 + S - Sr_0^{*2})q(1 + h_s^*) \ln r_0^*}{q(1 + h_s^*)(\ln r_1^* - \ln r_0^*) - q(\beta + h_s^*) \ln r_1^*}, \quad C_2 = -S$$

meanwhile, the expression of flow rate is deduced:

$$Q_0^* = \frac{(1 + S - Sr_0^{*2})q(1 + h_s^*)q(\beta + h_s^*)}{q(1 + h_s^*)(\ln r_1^* - \ln r_0^*) - q(\beta + h_s^*) \ln r_1^*} \tag{21}$$

Integrating the expression of pressure distribution with respect to r^* from 0 to 1, the expression of loading capacity is obtained:

$$W^* = \frac{W}{\pi R^2 P_s} = r_0^{*2} + 2 \left(\int_{r_0^*}^{r_1^*} r^* p_1^* dr^* + \int_{r_1^*}^1 r^* p_2^* dr^* \right) \tag{22}$$

3. Verification

To illustrate the validity of this discussion, a comparison between the results of this study and those of Dowson [34] is presented. By setting the values of non-Gaussian parameters kurtosis and skewness as $k = 3$ and $s = 0$, respectively, the bearing surface is changed into smooth. In this situation, the operation conditions of hydrostatic thrust bearings in this study are the same as those of Dowson [34]. Thus, the validity of derivation could be illustrated in this study if the results of this discussion agree with those of Dowson [34].

When the bearing surface is smooth, the values of $q(h^*)$ in the regions of bearing land and recess are:

$$q(\beta + h_s^*) = \beta^3, q(1 + h_s^*) = 1 \tag{23}$$

At this situation, the expressions of pressure distributions in Equations (19) and (20) are changed into:

$$p_1^* = 1 + S(r^{*2} - r_0^{*2}) - \frac{(1 + S - Sr_0^{*2})(\ln r^* - \ln r_0^*)}{(\ln r_1^* - \ln r_0^*) - \beta^3 \ln r_1^*} \quad r_0^* \leq r^* \leq r_1^* \tag{24}$$

$$p_2^* = S(r^{*2} - 1) - \frac{(1 + S - Sr_0^{*2})\beta^3 \ln r^*}{(\ln r_1^* - \ln r_0^*) - \beta^3 \ln r_1^*} \quad r_1^* \leq r^* \leq 1 \tag{25}$$

Substituting Equations (24) and (25) into Equation (22), the loading capacity of smooth bearings could be obtained; the results of this study were compared with those of Dowson [34], and the comparisons are displayed in Figure 2. It is found that the results of this study agree well with those of Dowson [34], which could illustrate the validity of this study.

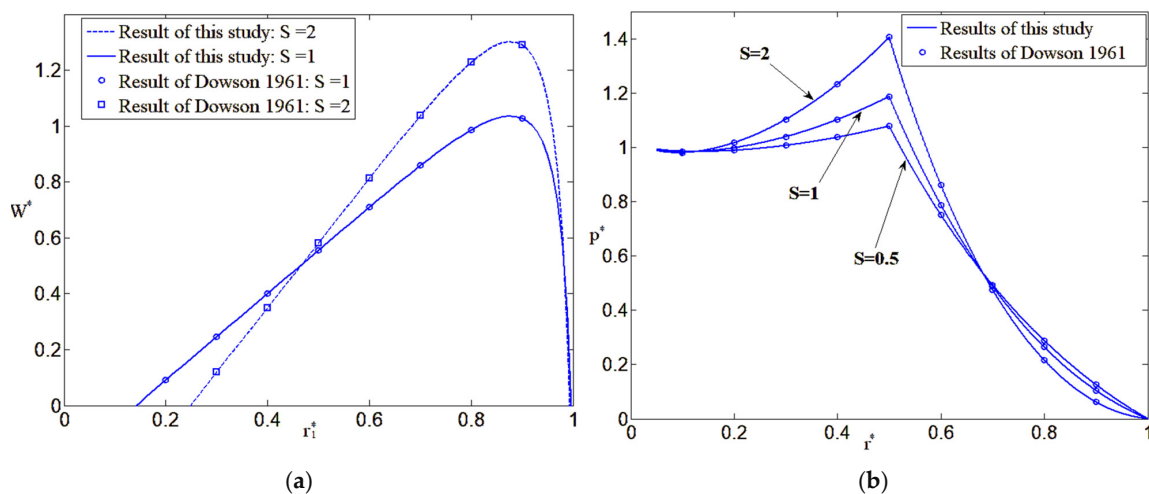


Figure 2. The comparisons between this study and a previous study [34]: (a) comparison of loading capacity; (b) comparison of pressure distribution.

4. Results and Discussion

The influence of non-Gaussian surface roughness on the static performance of hydrostatic bearings is discussed in this study. Two kinds of surface roughness are discussed in this section: circumferential roughness and radial roughness. In Figures 3 and 4, relationships between the non-Gaussian circumferential roughness and static performance of hydrostatic bearings are displayed. Additionally, the effects of the non-Gaussian radial roughness on the static performance of hydrostatic bearings are illustrated in Figures 5 and 6. The structure and running parameters of the bearing are: recess radius $r_1^* = 0.5$, depth parameter of recess $\beta = 2$, parameter of surface topography $c = 0.4$, value range of kurtosis k is 1~5, value range of skewness s is $-1.5 \sim 1.5$, and inertial parameter $S = 0, 1, 2$.

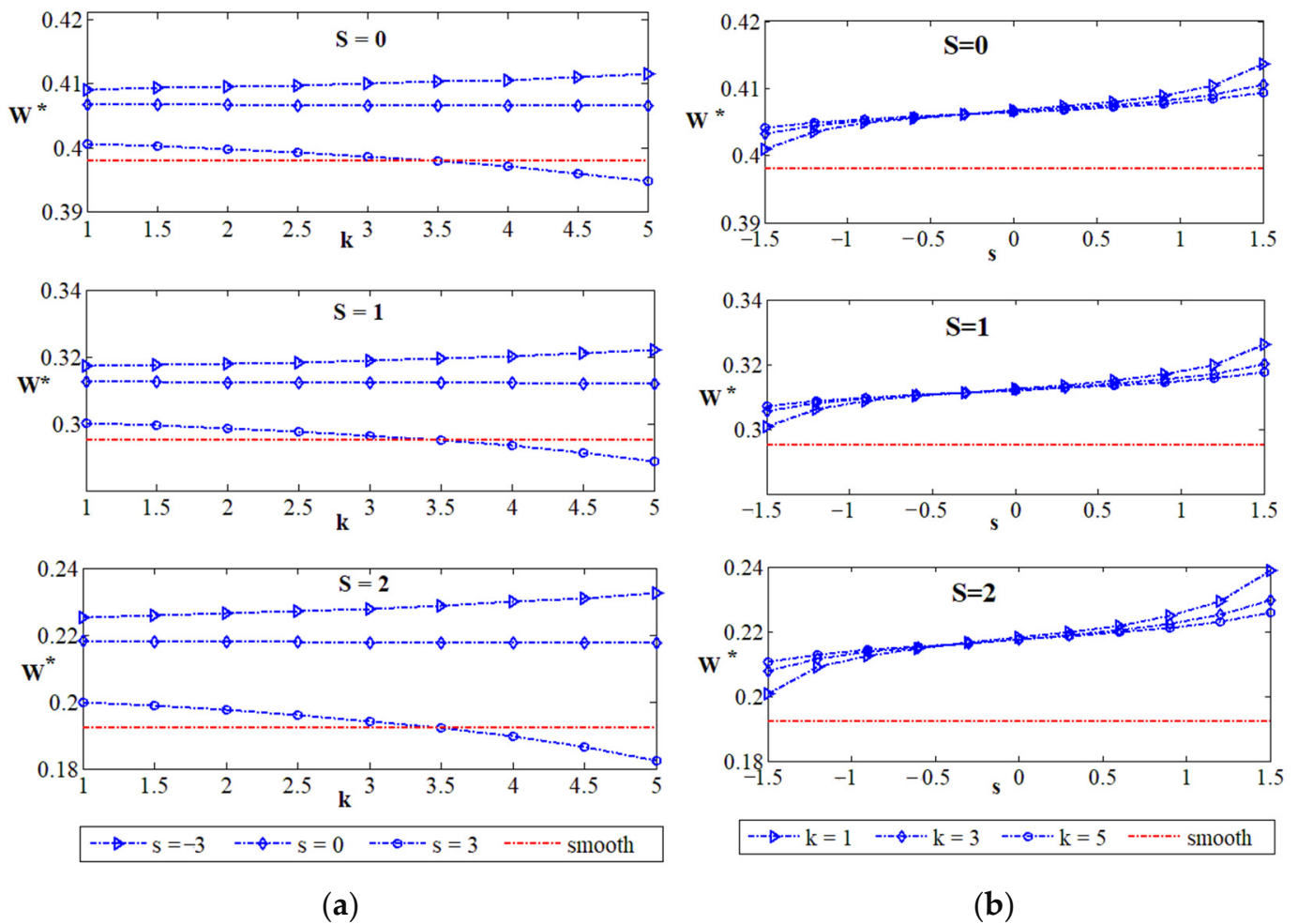


Figure 3. The influence of non-Gaussian circumferential roughness on the load capacity of hydrostatic thrust bearings: (a) kurtosis; (b) skewness.

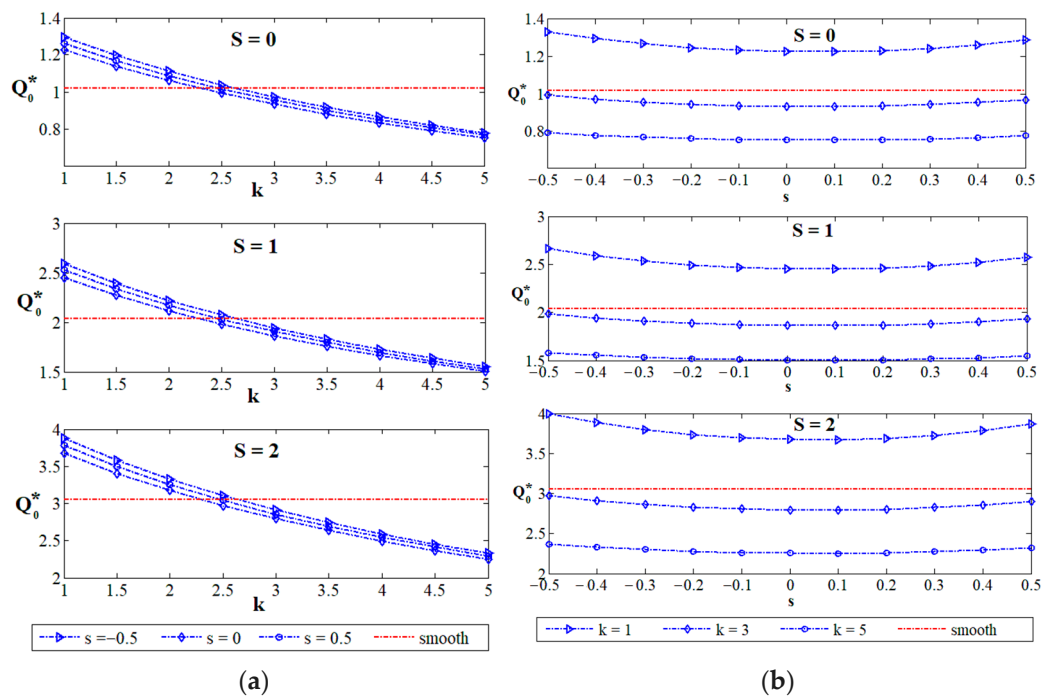


Figure 4. The influence of non-Gaussian circumferential roughness on the flow rate of hydrostatic thrust bearings: (a) kurtosis; (b) skewness.

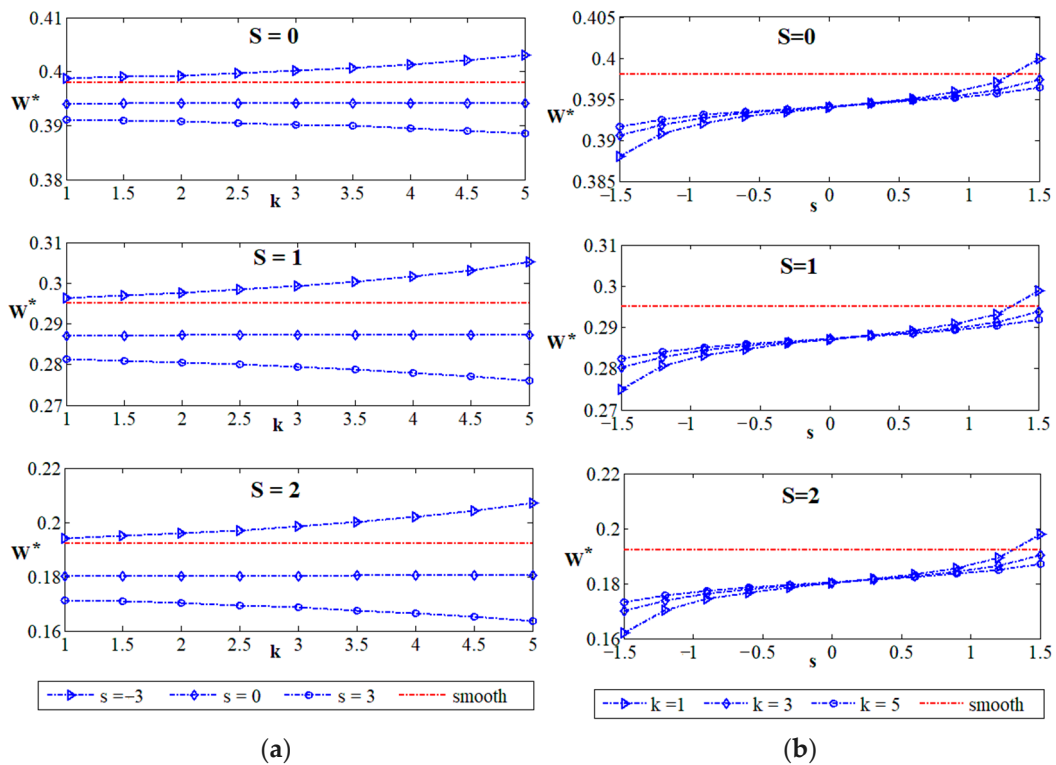


Figure 5. The influence of non-Gaussian radial roughness on the load capacity of hydrostatic thrust bearings: (a) kurtosis; (b) skewness.

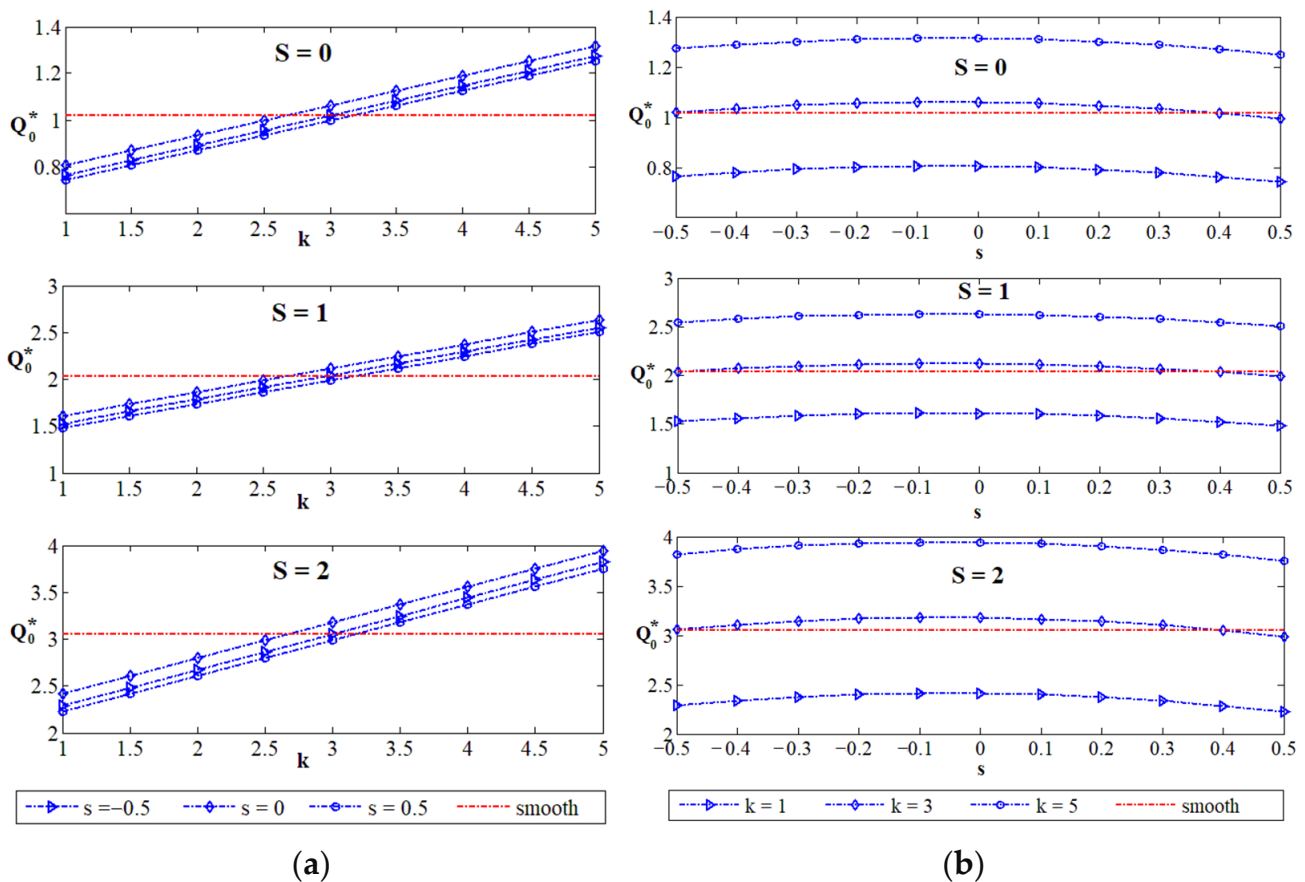


Figure 6. The influence of non-Gaussian radial roughness on the flow rate of hydrostatic thrust bearings: (a) kurtosis; (b) skewness.

The influence of the non-Gaussian circumferential roughness on the load capacity of hydrostatic thrust bearings is displayed in Figure 3. The relationship between the kurtosis of surface roughness and load capacity of the bearing is described in Figure 3a. For a negative skewness, the relationship between the load capacity and kurtosis is a positive correlation, while the relationship changes to a negative correlation with positive skewness. Additionally, the influence of kurtosis on load capacity is negligible when the value of skewness is 0. When the value of kurtosis varies from 1 to 5, the inertial parameter $S = 0$, the relative variations in load capacity are 0.61% ($s = -3$), 0.05% ($s = 0$), and -1.45% ($s = 3$); when the inertial parameter $S = 1$, the relative variations in load capacity are 1.54% ($s = -3$), 0.16% ($s = 0$), and -3.90% ($s = 3$); when the inertial parameter $S = 2$, the relative variations in load capacity are 3.24% ($s = -3$), 0.32% ($s = 0$), and -8.70% ($s = 3$). The influence of kurtosis on load capacity is enhanced with the increase in inertial parameter S . Compared with the situation of the Gaussian surface roughness model (i.e., $k = 3, s = 0$), for the non-Gaussian parameters $k = 5$ and $s = 3$, when inertial parameter $S = 0, 1, 2$, the calculation errors of load capacity between the results of Gaussian and non-Gaussian surface roughness are 2.90%, 7.56%, and 13.79%, respectively; for the non-Gaussian parameters $k = 5$ and $s = -3$, when inertial parameter $S = 0, 1, 2$, the calculation errors of load capacity between the results of the Gaussian and non-Gaussian model are 1.23%, 3.50%, and 6.84%, respectively. The relationship between the skewness of non-Gaussian surface roughness and load capacity of the bearing is displayed in Figure 3. The relationship between load capacity and kurtosis is a positive correlation, and the gradient of the variation curve decreases with the increase in kurtosis. At the region around $s = 0$, the influence of kurtosis on the load capacity is negligible, which agrees with the results in Figure 3a. When the value of skewness varies from -1.5 to 1.5 , the inertial parameter $S = 0$ and the relative variations in load capacity

are 3.17% ($k = 1$), 1.81% ($k = 3$), and 1.26% ($k = 5$); when the inertial parameter $S = 1$, the relative variations of load capacity are 8.44% ($k = 1$), 4.74% ($k = 3$), 3.35% ($k = 5$); when the inertial parameter $S = 2$, the relative variations in load capacity are 18.89% ($k = 1$), 10.54% ($k = 3$), 7.32% ($k = 5$). In other words, with the increase in inertial parameter S , the influence of skewness on load capacity is enhanced. The reason the load carrying capacity of bearings is enhanced by the topology surface is as follows: when the lubricant flows through the topology surface, the rough surface of the bearing slows down the flow of lubricant, and the dented region of the bearing surface can store a portion of the energy from the flowing lubricant. This stored energy can support a portion of the load. Consequently, bearings with a topology surface have a higher load carrying capacity compared with smooth bearings.

The influence of non-Gaussian circumferential roughness on the flow rate of hydrostatic thrust bearings is displayed in Figure 4. The relationship between the kurtosis of surface roughness and flow rate of the bearing is described in Figure 4a. It could be found that the relationship between flow rate and kurtosis is negative correlation obviously, and the gradient of the variation curve is decrescent with the increasing of kurtosis. Different from the situation of load capacity, the relative variations in flow rate are not affected by the varying of inertial parameter S . During the value of kurtosis varying from 1 to 5, the relative variations in flow rate are $-40.00%$ ($s = -0.5$), $-38.69%$ ($s = 0$), $-39.38%$ ($s = 0.5$). Comparing with the results of Gaussian surface roughness model (i.e., $k = 3, s = 0$): for the non-Gaussian parameters $k = 5$ and $s = 0.5$, the calculation error of flow rate between the results of the Gaussian and non-Gaussian models is 17.89%, while for the non-Gaussian parameters $k = 5$ and $s = -0.5$, the calculation error of flow rate between the results of Gaussian and non-Gaussian models is 16.60%. The relationship between the skewness of non-Gaussian surface roughness and flow rate of the bearing is described in Figure 4b. With the increase in skewness, the value of the flow rate first decreased then increased, and reached the minimum at $s = 0$. For a larger value of kurtosis, the amplitude of variation was smaller.

The influence of non-Gaussian radial roughness on the load capacity of hydrostatic thrust bearings is displayed in Figure 5. The relationship between the kurtosis of non-Gaussian surface roughness and load capacity of the bearing is described in Figure 5a. For negative skewness, the relationship between load capacity and kurtosis is a positive correlation, while the relationship changes to be negative correlation with a positive skewness. Additionally, the influence of kurtosis on load capacity is negligible when the value of skewness is 0. When the value of kurtosis varies from 1 to 5, the inertial parameter $S = 0$, the relative variations in load capacity are 0.61% ($s = -3$), 0.03% ($s = 0$), and $-0.66%$ ($s = 3$); when the inertial parameter $S = 1$, the relative variations in load capacity are 2.97% ($s = -3$), 0.07% ($s = 0$), and $-1.88%$ ($s = 3$); when the inertial parameter $S = 2$, the relative variations in load capacity are 6.80% ($s = -3$), 0.22% ($s = 0$), and $-4.61%$ ($s = 3$). The influence of kurtosis on load capacity is enhanced with the increasing of inertial parameter S . Compared with the situation of the Gaussian surface roughness model (i.e., $k = 3, s = 0$): for the non-Gaussian parameters $k = 5, s = 3$, when inertial parameter $S = 0, 1, 2$, the calculation errors of load capacity between the results of Gaussian and non-Gaussian models are 1.42%, 3.90%, and 9.32%, respectively; for the non-Gaussian parameters $k = 5$ and $s = -3$, when inertial parameter $S = 0, 1, 2$, the calculation errors of load capacity between the results of Gaussian and non-Gaussian models are 2.28%, 6.27%, and 14.98%, respectively. The relationship between the skewness of non-Gaussian surface roughness and load capacity of the bearing is displayed in Figure 5b. The relationship between load capacity and kurtosis is a positive correlation, and the gradient of the variation curve decreases with the increase in kurtosis. For the region around $s = 0$, the influence of kurtosis on load capacity is negligible, which agrees with the results in Figure 5a. When the value of skewness varies from -1.5 to 1.5 , the inertial parameter $S = 0$, the relative variations in load capacity are 3.07% ($k = 1$), 1.74% ($k = 3$), and 1.20% ($k = 5$); when the inertial parameter $S = 1$, the relative variations in load capacity are 8.69% ($k = 1$), 4.85% ($k = 3$), and 3.36% ($k = 5$); when the inertial parameter

$S = 2$, the relative variations in load capacity are 22.02% ($k = 1$), 11.95% ($k = 3$), and 8.20% ($k = 5$). In other words, with the increases in inertial parameter S , the influence of skewness on load capacity is enhanced.

The influence of non-Gaussian radial roughness on the flow rate of hydrostatic thrust bearings is displayed in Figure 6. The relationship between the kurtosis of non-Gaussian surface roughness and flow rate of the bearing is described in Figure 6a. The relationship between the flow rate and kurtosis is clearly a positive correlation, and the gradient of the variation curve is nearly invariable with the increase in kurtosis. Different from the situation of load capacity, the relative variations in flow rate are not affected by varying the inertial parameter, S . During the value of kurtosis varying from 1 to 5, the relative variations in flow rate are 66.70% ($s = -0.5$), 63.71% ($s = 0$), and 68.76% ($s = 0.5$). Compared with the results of the Gaussian surface roughness model (i.e., $k = 3$, $s = 0$), for the non-Gaussian parameters $k = 5$ and $s = 0.5$, the calculation error of flow rate between the results of Gaussian and non-Gaussian model is 18.06%, while for the non-Gaussian parameters $k = 5$ and $s = -0.5$, the calculation error of flow rate between the results of Gaussian and non-Gaussian model is 20.22%. The relationship between the skewness of non-Gaussian surface roughness and flow rate of the bearing is displayed in Figure 6b. With the increase in skewness, the value of flow rate first increased then decreased, and reached the maximum at $s = 0$.

5. Conclusions

By bringing in the Edgeworth expansion, the non-Gaussian distribution model of surface topography was established for hydrostatic thrust bearing in this study. The non-Gaussian distribution of bearing surface topography is characterized by two parameters: kurtosis, k , and skewness, s .

For the static performance of hydrostatic thrust bearings, it was found that the calculation error between the results of the Gaussian distribution model and that of the non-Gaussian distribution model can reach more than 10%, and the error between the two models would be greater for bearings with a higher rotating speed.

The actual distribution of bearing surface topography was non-Gaussian; therefore, the application of the Gaussian model would clearly produce errors during discussion of the static characteristics of hydrostatic thrust bearings considering the surface topography. Therefore, the non-Gaussian distribution model should be applied. Moreover, the non-Gaussian parameters (kurtosis, k , and skewness, s) of the bearing surface topography can significantly affect the static characteristics of hydrostatic thrust bearing. Thus, to improve the static characteristics of hydrostatic thrust bearings, the bearing surface can be machined into a specific non-Gaussian distribution by adjusting the angle and feed mode of cutting tools during the machining process of the bearing.

Author Contributions: Methodology, Z.T.; formal analysis, Z.T.; investigation, H.L.; writing—original draft preparation, Z.T.; writing—review and editing, H.L. All authors have read and agreed to the published version of the manuscript.

Funding: This study was supported by National Key Research and Development Program of China (No. 2020YFB2007600), Science Challenge Project (No. TZ2018006-0102-03) and Central government guides local science and technology development projects of Hubei Province (No. 2018ZYD016), R&D Project of Xiangyang.

Data Availability Statement: Not applicable.

Conflicts of Interest: The authors declare no conflict of interest. The funders had no role in the design of the study; in the collection, analyses, or interpretation of data; in the writing of the manuscript; or in the decision to publish the results.

References

1. Tian, Z.X.; Cao, H.Y.; Huang, Y. Static characteristics of hydrostatic thrust bearing considering the inertia effect on the region of supply hole. *Proc. Inst. Mech. Eng. Part J J. Eng. Tribol.* **2019**, *233*, 188–193. [[CrossRef](#)]
2. Shang, Y.; Cheng, K.; Ding, H.; Chen, S. Design of a Hydrostatic Spindle and Its Simulation Analysis with the Application to a High Precision Internal Grinding Machine. *Machines* **2022**, *10*, 127. [[CrossRef](#)]
3. Huang, H.C.; Yang, W.H. Thermal Characteristics of a Vertical Hydrostatic Guideway System for Precision Milling Machine Applications. *Lubricants* **2022**, *10*, 247. [[CrossRef](#)]
4. Song, L.; Cheng, K.; Ding, H.; Chen, S.; Gao, Q. Analysis of static and dynamic characteristics of spiral-grooved gas journal bearings in high speed. *Proc. Inst. Mech. Eng. Part C J. Mech. Eng. Sci.* **2019**, *233*, 6774–6792. [[CrossRef](#)]
5. Feng, H.; Gao, Z.; van Ostayen, R.A.J.; Zhang, X. A Numerical Investigation of the Effects of Groove Texture on the Dynamics of a Water-Lubricated Bearing–Rotor System. *Lubricants* **2023**, *11*, 242. [[CrossRef](#)]
6. Christensen, H. Stochastic Models for Hydrodynamic Lubrication of Rough Surfaces. *Proc. Inst. Mech. Eng.* **1969**, *184*, 1013–1026. [[CrossRef](#)]
7. Lin, J.R. Surface roughness effect on the dynamic stiffness and damping characteristics of compensated hydrostatic thrust bearings. *Int. J. Mach. Tools Manuf.* **2000**, *40*, 1671–1689. [[CrossRef](#)]
8. Walicka, A.; Walicki, E.; Jurczak, P.; Falicki, J. Thrust Bearing with Rough Surfaces Lubricated by an Ellis Fluid. *Int. J. Appl. Mech. Eng.* **2014**, *19*, 809–822. [[CrossRef](#)]
9. Walicka, A.; Walicki, E.; Jurczak, P.; Falicki, J. Curvilinear squeeze film bearing with rough surfaces lubricated by a Rabinowitsch–Rotem–Shinnar fluid. *Appl. Math. Model.* **2016**, *40*, 7916–7927. [[CrossRef](#)]
10. Walicka, A. Porous curvilinear squeeze film bearing with rough surfaces lubricated by a power-law fluid. *J. Porous Media* **2012**, *15*, 29–49. [[CrossRef](#)]
11. Lin, J.R. Application of the Hopf bifurcation theory to limit cycle prediction of short journal bearings with isotropic roughness effects. *Proc. Inst. Mech. Eng. Part J J. Eng. Tribol.* **2007**, *221*, 869–879. [[CrossRef](#)]
12. Lin, J.R. The surface roughness effects of transverse patterns on the Hopf bifurcation behaviors of short journal bearings. *Ind. Lubr. Tribol.* **2012**, *64*, 265–270. [[CrossRef](#)]
13. Lin, J.R. The influences of longitudinal surface roughness on sub-critical and super-critical limit cycles of short journal bearings. *Appl. Math. Model.* **2014**, *38*, 392–402. [[CrossRef](#)]
14. Naduvinamani, N.B.; Hiremath, P.S.; Gurubasavaraj, G. Effect of surface roughness on the static characteristics of rotor bearings with couple stress fluids. *Comput. Struct.* **2002**, *80*, 1243–1253. [[CrossRef](#)]
15. Bujurke, N.M.; Naduvinamani, N.B.; Basti, D.P. Effect of surface roughness on the squeeze film lubrication between curved annular plates. *Ind. Lubr. Tribol.* **2007**, *59*, 178–185. [[CrossRef](#)]
16. Naduvinamani, N.B.; Fathima, S.T.; Jamal, S. Effect of roughness on hydromagnetic squeeze films between porous rectangular plates. *Tribol. Int.* **2010**, *43*, 2145–2151. [[CrossRef](#)]
17. Naduvinamani, N.B.; Gurubasavaraj, G. Surface roughness effects on squeeze films in curved circular plates. *Ind. Lubr. Tribol.* **2004**, *56*, 346–352. [[CrossRef](#)]
18. Jurczak, P.; Falicki, J. Pressure Distribution in a Squeeze Film Spherical Bearing with Rough Surfaces Lubricated by an Ellis Fluid. *Int. J. Appl. Mech. Eng.* **2016**, *21*, 593–610. [[CrossRef](#)]
19. Zhang, G.; Li, J.; Tian, Z.; Huang, Y.; Chen, R. Film shape optimization for two-dimensional rough slider bearings. *Tribol. Trans.* **2016**, *59*, 17–27. [[CrossRef](#)]
20. Lin, J.R.; Hung, T.C.; Chou, T.L.; Liang, L.J. Effects of surface roughness and non-Newtonian micropolar fluids on dynamic characteristics of wide plane slider bearings. *Tribol. Int.* **2013**, *66*, 150–156. [[CrossRef](#)]
21. Pang, G.; Qi, X.; Ma, Q.; Zhao, X.; Wen, C.; Xu, W.; Peng, Y. Surface roughness and roundness of bearing raceway machined by floating abrasive polishing and their effects on bearing’s running noise. *Chin. J. Mech. Eng.* **2014**, *27*, 543–550. [[CrossRef](#)]
22. Tian, Z.; Chen, G. Discussion on dynamic characteristics of long journal bearings considering surface roughness. *Adv. Mech. Eng.* **2022**, *14*, 16878132221136451. [[CrossRef](#)]
23. Pei, S.; Xu, H.; Yun, M.; Shi, F.; Hong, J. Effects of surface texture on the lubrication performance of the floating ring bearing. *Tribol. Int.* **2016**, *102*, 143–153. [[CrossRef](#)]
24. Peklenik, J. New developments in surface characterisation and measurements by means of random process analysis. *Proc. Inst. Mech. Eng.* **1967**, *182*, 108–126.
25. Li, J.; Zhang, G.; Huang, Y.; Chen, R.; Yan, S.; Cao, H. Influence of non-Gaussian-distributed surface roughness on the static performance of slider bearings. *Tribol. Trans.* **2016**, *60*, 739–752. [[CrossRef](#)]
26. Tian, Z.; Li, B. Threshold speed of short journal bearings considering the non-Gaussian longitudinal surface roughness. *Proc. Inst. Mech. Eng. Part J J. Eng. Tribol.* **2022**, *236*, 2138–2145. [[CrossRef](#)]
27. Winkler, A.; Bartz, M.; Wartzack, S. Numerical Wear Modeling in the Mixed and Boundary Lubrication Regime. *Lubricants* **2022**, *10*, 334. [[CrossRef](#)]
28. Ma, J.; Fu, C.; Zhang, H.; Chu, F.; Shi, Z.; Gu, F.; Ball, A.D. Modelling non-Gaussian surfaces and misalignment for condition monitoring of journal bearings. *Measurement* **2021**, *174*, 108983. [[CrossRef](#)]
29. Pei, J.; Han, X.; Tao, Y.; Feng, S. Mixed elastohydrodynamic lubrication analysis of line contact with Non-Gaussian surface roughness. *Tribol. Int.* **2020**, *151*, 106449. [[CrossRef](#)]

30. Chen, J.; Liu, D.; Wang, C.; Zhang, W.; Zhu, L. A fractal contact model of rough surfaces considering detailed multi-scale effects. *Tribol. Int.* **2022**, *176*, 107920. [[CrossRef](#)]
31. Ren, J.; Yuan, H. Contact Analysis and Friction Prediction of Non-Gaussian Random Surfaces. *Appl. Sci.* **2022**, *12*, 11237. [[CrossRef](#)]
32. Zhao, J.; Li, Z.; Zhang, H.; Zhu, R. Prediction of the tribological characteristics of non-Gaussian rough surfaces during sliding wear in mixed lubrication. *Lubr. Sci.* **2022**, *34*, 127–139. [[CrossRef](#)]
33. Jondeau, E.; Rockinger, M. Gram–Charlier densities. *J. Econ. Dyn. Control.* **2001**, *25*, 1457–1483. [[CrossRef](#)]
34. Dowson, D. Inertia effects in hydrostatic thrust bearings. *J. Fluids Eng.* **1961**, *83*, 227–234. [[CrossRef](#)]

Disclaimer/Publisher’s Note: The statements, opinions and data contained in all publications are solely those of the individual author(s) and contributor(s) and not of MDPI and/or the editor(s). MDPI and/or the editor(s) disclaim responsibility for any injury to people or property resulting from any ideas, methods, instructions or products referred to in the content.